

Theoretical investigations on radiative opacity of OsO: Contributions from the multiplet states

Wen Yan(严汶), Yong Hou(侯永), Feng-Tao Jin(靳奉涛), Cheng Gao(高城), Jiao-Long Zeng(曾交龙), and Jian-Min Yuan(袁建民)

Citation: Chin. Phys. B, 2026, 35 (**8**): 089701. DOI: 10.1088/1674-1056/ae7057
http://cpb.iphy.ac.cn; http://iopscience.iop.org/cpb

What follows is a list of articles you may be interested in

Spectroscopy and molecule opacity investigation on excited states of SiS

Rui Li(李瑞), Haonan Lv(吕浩男), Jiqun Sang(桑纪群), Xiaohua Liu(刘晓华), Guiying Liang(梁桂颖), and Yong Wu(吴勇)

Chin. Phys. B, 2024, 33 (**5**): 053101. DOI: 10.1088/1674-1056/ad20dc

Low-lying electronic states of osmium monoxide OsO

Wen Yan(严汶) and Wenli Zou(邹文利)

Chin. Phys. B, 2023, 32 (**11**): 113101. DOI: 10.1088/1674-1056/acec46

Molecule opacity study on low-lying states of CS

Rui Li(李瑞), Jiqun Sang(桑纪群), Xiaohe Lin(林晓贺), Jianjun Li(李建军), Guiying Liang(梁桂颖), and Yong Wu(吴勇)

Chin. Phys. B, 2022, 31 (**10**): 103101. DOI: 10.1088/1674-1056/ac834f

Highly accurate theoretical study on spectroscopic properties of SH including spin-orbit coupling

Shu-Tao Zhao(赵书涛), Xin-Peng Liu(刘鑫鹏), Rui Li(李瑞), Hui-Jie Guo(国慧杰), and Bing Yan(闫冰)

Chin. Phys. B, 2021, 30 (**7**): 073104. DOI: 10.1088/1674-1056/ac003f

Configuration interaction study on low-lying states of AlCl molecule

Xiao-Ying Ren(任笑影), Zhi-Yu Xiao(肖志宇), Yong Liu(刘勇), and Bing Yan(闫冰)

Chin. Phys. B, 2021, 30 (**5**): 053101. DOI: 10.1088/1674-1056/abd46a

---

DATA PAPER

Theoretical investigations on radiative opacity of OsO: Contributions from the multiplet states

Wen Yan(严汶)[1], Yong Hou(侯永)[1], Feng-Tao Jin(靳奉涛)[1], Cheng Gao(高城)[1,†], Jiao-Long Zeng(曾交龙)[2], and Jian-Min Yuan(袁建民)[3]

[1] *College of Science, National University of Defense Technology, Changsha* 410073, *China*
[2] *College of Science, Zhejiang University of Technology, Hangzhou* 310023, *China*
[3] *Institute of Atomic and Molecular Physics, Jilin University, Changchun* 130012, *China*

(Received 3 March 2026; revised manuscript received 26 April 2026; accepted manuscript online 20 May 2026)

We report the first high-precision opacity calculations for osmium monoxide (OsO) over a wide temperature range (300–5000 K). Using a high-level relativistic electronic structure method, we generated a comprehensive line list from the 12 low-lying electronic states. The strong spin-orbit coupling effect in OsO leads to a near-degeneracy between the ground $X^1\Sigma^+$ state and the first excited $a^3\Pi$ state. This results in a complex composite spectrum where triplet transitions contribute predominantly in the near ultraviolet region. At high temperatures, the high-density quintet transitions blend to form a distinctive quasi-continuous absorption background in the ultraviolet region. This study fills a critical gap for heavy transition-metal oxides in spectroscopic databases, and is helpful for detecting and diagnosing r-process elements in astronomical spectra. The datasets presented in this paper, including the complete line lists and absorption cross-sections for OsO at temperatures from 300 K to 5000 K, are openly available at https://www.doi.org/10.57760/sciencedb.j00113.00282.

Keywords: radiative opacity, osmium monoxide, line list

PACS: 97.10.Ex, 31.50.Df, 31.15.ag, 31.15.aj

DOI: 10.1088/1674-1056/ae7057 **CSTR:** 32038.14.CPB.ae7057

1. Introduction

Radiative opacity plays a significant role in astrophysics, which determines the stellar structure and chemical evolution.[1,2] For high temperature plasmas in the solar interior, radiative opacity is predominantly caused by atomic absorption.[3,4] For relatively low temperature astronomical objects such as brown dwarfs, M/L-type dwarfs, and hot exoplanets, molecular absorptions are the most important contributions to radiative opacity.[5,6] Compared with atomic opacity, molecular opacity is more complicated, which is composed of rotation, vibration, and electronic transitions. Accurate determination of molecular opacity is a challenge.

Radiative opacity of heavy metal oxides is essential for simulating astronomical observations and understanding the physical properties of stellar physics. The heavy elements are predominantly synthesized via the rapid neutron-capture process (r-process), which operates in extreme neutron-rich environments such as neutron-star mergers.[7] Infrared and optical observations of r-process-enriched objects, e.g., metal-poor stars and kilonova remnants, reveal absorption features that likely contain contributions from heavy-element molecules.[8,9] Osmium (Os) is a key element located near the third r-process peak; its abundance pattern provides strong constraints on nucleosynthesis models. A precise interpretation of these observations in the r-process, and their translation into quantitative constraints on nucleosynthesis physics, urgently requires accurate radiative opacity of molecules.

There have been some molecular databases,[10–15] providing extensive energy levels and radiative data for light molecules. However, the electronic structures of OsO pose formidable challenges for high-accuracy calculations. The Os atom in OsO possesses an open 5d shell. For such heavy elements, relativistic effects and spin–orbit coupling play a significant role in determining the electronic structure.[16] The combination of these effects with the inherent degeneracy of d orbitals results in a dense manifold of low-lying electronic states. Consequently, spectral data for OsO molecules remain absent from major spectroscopic databases (e.g., ExoMol,[17,18] HITRAN,[19,20] and GEISA[21,22]).

In this work, we systematically investigate the radiative opacity of OsO across a broad temperature range of 300–5000 K. The potential energy curves (PECs), energy levels, transition and permanent dipole moments for the 12 low-lying electronic states of OsO are obtained by using a high-level relativistic quantum chemical method, in which effects of spin-orbit couplings and electronic angular momentum couplings are considered. Beyond filling a critical gap in spectroscopic databases, this study provides the foundational data required for future spectroscopic diagnostics that may quantitatively reveal the physical and chemical conditions of r-process products in astronomical environments.

[†]Corresponding author. E-mail: gaocheng@nudt.edu.cn

© 2026 Chinese Physical Society and IOP Publishing Ltd. All rights, including for text and data mining, AI training, and similar technologies, are reserved.

2. Data acquisition and processing methods

Under local thermodynamic equilibrium (LTE), the radiative opacity (absorption cross-section) at wavenumber $\tilde{\nu}$ is expressed as

$$\sigma(\tilde{\nu}) = \sum_{f,i} I(f \leftarrow i)\, f^{\mathrm{V}}(\tilde{\nu}), \tag{1}$$

where $I(f \leftarrow i)$ denotes the line intensity for a transition $f \leftarrow i$, and f^{V} is the line profile taken as a Voigt one.[23]

The line intensity for a given transition under LTE conditions is calculated as

$$I(f \leftarrow i) = \frac{g_f^{\mathrm{tot}} A_{fi}}{8\pi c \tilde{\nu}_{fi}^2} \frac{\mathrm{e}^{-c_2 \tilde{E}_i/T}\left(1 - \mathrm{e}^{-c_2 \tilde{\nu}_{fi}/T}\right)}{Q(T)}, \tag{2}$$

where $g_f^{\mathrm{tot}} = g_f^{\mathrm{ns}}(2J_f + 1)$ is the total degeneracy of the upper state, $c_2 = hc/k_{\mathrm{B}}$, and $Q(T)$ is the partition function.[24]

The Einstein spontaneous emission coefficient A_{fi} is expressed as

$$A_{fi} = \frac{64 \times 10^{-36}\pi^4}{3h}(2J_i + 1)\tilde{\nu}^3 \sum_{\substack{t=-1,\\ 0,1}} \left| \sum_{\substack{n_i,\\ n_f}} \left(C_{\lambda_f, n_f}^{J_f, \tau_f}\right)^* C_{\lambda_i, n_i}^{J_i, \tau_i} \times (-1)^{\Omega_i} \begin{pmatrix} J_i & 1 & J_f \\ \Omega_i & t & -\Omega_f \end{pmatrix} \langle v_f | \bar{\mu}_t^{f,i}(r) | v_i \rangle \right|^2. \tag{3}$$

Here, $\bar{\mu}_t$ are the irreducible components of the electric dipole moment, and $C_{\lambda,n}^{J,\tau}$ are the expansion coefficients of the rovibronic wave functions, which are eigenfunctions of the total molecular Hamiltonian including the electronic, vibrational, rotational, spin-orbit, spin-rotation, spin-spin, and Λ-type doubling terms.[25–27]

The rovibronic energy levels and wave functions used in the above expressions were generated by solving the coupled-channel Schrödinger equation for nuclear motion using a variational approach, taking into account the non-adiabatic couplings among multiple electronic states. The molecular electronic structure data — PECs, spin–orbit couplings, electronic angular momentum couplings, and transition and permanent dipole moments for 12 electronic states of OsO — were computed with high-level relativistic quantum chemical methods. Specifically, we employed the exact two-component (X2C) Hamiltonian[16,28] combined with the ANO-R3 basis set[29,30] and the multi-reference MS-NEVPT2 method[31] as implemented in the BDF software package.[32] The details of these electronic structure calculations are available in our earlier work.[33] The PECs were computed over an internuclear distance range of approximately 1.5–2.2 Å, which adequately covers the Franck–Condon region relevant for the bound-bound transitions considered in this work. At the temperatures of interest ($\leq$ 5000 K), the vibrational wavefunctions of populated levels have negligible amplitude at larger internuclear distances, ensuring that the computed bound–bound opacities are insensitive to the truncation of the PECs.

3. Data format and contents of the database

The complete dataset is organized into two primary file types: state files and transition files, adhering to the standard format widely used in molecular spectroscopy.[34]

Table 1. Excerpt from the OsO states file, using the format defined by Tennyson.[34] The complete file is openly available in the Science Data Bank (see Data availability statement).

n	E	g_{tot}	J	τ	$p_{+/-}$	$p_{e/f}$	State	v	Λ	Σ	Ω	Source
3	1121.784856	1	0	9.4100E − 02	+	e	$X^1\Sigma^+$	1	0	0	0	Ca
7	2232.548158	1	0	4.7763E − 02	+	e	$X^1\Sigma^+$	2	0	0	0	Ca
10	3334.638434	1	0	3.2193E − 02	+	e	$X^1\Sigma^+$	3	0	0	0	Ca
13	4430.301549	1	0	2.4317E − 02	+	e	$X^1\Sigma^+$	4	0	0	0	Ca
16	5525.390677	1	0	1.9410E − 02	+	e	$X^1\Sigma^+$	5	0	0	0	Ca

Note: n: state index; E: energy (in cm^{-1}); g_{tot}: total degeneracy; J: total angular momentum; τ: lifetime (in s); $p_{+/-}$: total parity; $p_{e/f}$: rotationless parity; state: electronic state; v: vibrational quantum number; Λ: projection of $\hat{\boldsymbol{L}}$ along internuclear axis; Σ: projection of $\hat{\boldsymbol{S}}$ along internuclear axis; Ω: projection of $\hat{\boldsymbol{J}}$ along internuclear axis ($\Omega = \Lambda + \Sigma$); Source: state source (Ma, EH or Ca).

Table 1 shows a sample of the state file. Each row corresponds to a unique rovibronic state, identified by a sequential index n. For each state, we provide its energy term value E (in cm^{-1}), total degeneracy g_{tot}, total angular momentum J, lifetime τ, and the associated quantum numbers including parity, electronic state, vibrational quantum number, and the projections Λ, Σ, and Ω. The final column indicates the source of the state (e.g., calculated in this work, 'Ca').

Table 2 presents a sample of the transition file. Each row represents an electric dipole allowed transition between an initial state i and a final state f (referencing the indices n from the state file), accompanied by the Einstein A coefficient for spontaneous emission.

Table 2. Excerpt from the OsO trans file, using the format defined by Tennyson, Hill.[34] The complete file is openly available in the Science Data Bank (see Data availability statement).

f	i	A_f (s^{-1})
1094	1	2.1037E + 03
1053	7	1.7698E + 03
1389	16	1.4141E + 03

4. Results and discussion

The rovibronic spectrum of OsO is characterized by its rich manifold of low-lying electronic states. In this work, we have computed 12 Λ–S states encompassing singlets, triplets, and quintets, namely, $X^1\Sigma^+$ ($[1]^1\Sigma^+$), $A^1\Sigma^+$ ($[2]^1\Sigma^+$), $B^1\Sigma^+$ ($[3]^1\Sigma^+$), $a^3\Pi$ ($[1]^3\Pi$), $b^3\Pi$ ($[2]^3\Pi$), $c^3\Pi$ ($[3]^3\Pi$), $d^3\Pi$ ($[4]^3\Pi$), $A^5\Pi$ ($[1]^5\Pi$), $B^5\Pi$ ($[2]^5\Pi$), $C^5\Pi$ ($[3]^5\Pi$), $A^5\Delta$ ($[1]^5\Delta$), and $B^5\Delta$ ($[2]^5\Delta$). The adiabatic excitation energies and potential energy curves of these states are presented in Figs. 1 and 2, respectively.

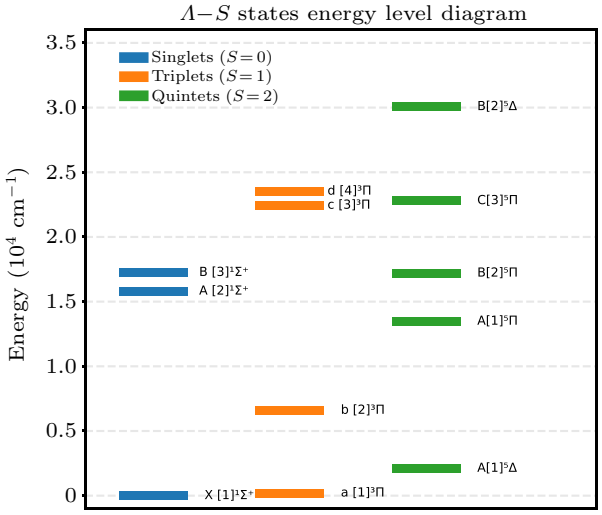


Fig. 1. Adiabatic excitation energies of the 12 low-lying OsO electronic states.

This dense and multiplicity-diverse low-energy electronic structure presages an extremely complex band system for OsO. It is particularly noteworthy that the $a^3\Pi$ state lies exceptionally low in energy, being nearly degenerate with the $X^1\Sigma^+$ state (see Fig. 1). Previous studies (see, e.g., Ref. [33]) have shown that, when spin–orbit coupling is taken into account, the $a^3\Pi$ state effectively assumes the primary character of the ground state, contributing approximately 83% of its wavefunction composition. Consequently, even at low temperature, the $a^3\Pi$ state possesses a significant population. To further appreciate the role of spin–orbit coupling, it is instructive to contrast the present Ω-state spectrum with a hypothetical scalar-relativistic (Λ–S) spectrum. Without SOC, the ground state would be the closed-shell $X^1\Sigma^+$ state, and transitions from the low-lying $a^3\Pi$ state would appear only as hot bands. The strong SOC in OsO not only inverts the energetic ordering but also heavily mixes the singlet and triplet manifolds. As a result, the $\{1\}2$ ground Ω state possesses $\sim 83\%$ $a^3\Pi$ character, activating a dense network of triplet-dominated transitions that would otherwise be weak or absent. This mixing, combined with the SOC splitting of the quintet states, is directly responsible for the complex temperature-dependent opacity revealed in Figs. 3 and 4. According to Boltzmann statistics, across a wide temperature range, the molecular population will be predominantly distributed between these two lowest-lying states, $a^3\Pi$ and $X^1\Sigma^+$. Therefore, transitions originating from these two states collectively weave the intricate spectral tapestry of OsO. The allowed transitions from these low-lying reservoirs are expected to produce prominent absorption features spanning from the visible to the near-infrared region.

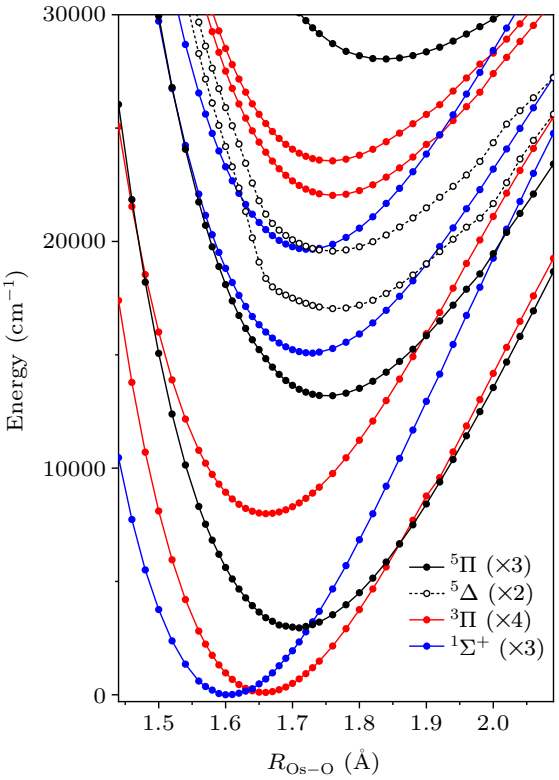


Fig. 2. Potential energy curves of the 12 low-lying OsO electronic states.

In Fig. 3, the total OsO absorption cross section at 2000 K is decomposed into its primary contributing electronic transitions across the calculated spectral range (0–40000 cm^{-1}). The spectrum reveals a high degree of complexity, with significant opacity contributions spanning from the infrared to the far-ultraviolet, a direct consequence of the dense, low-lying electronic manifold encompassing singlet, triplet, and quintet states.

The absorption features can be delineated into distinct spectral regions based on the dominant transitions. In the far-infrared to mid-infrared region of 0–4200 cm^{-1} (Fig. 3(a)), the opacity is primarily due to vibration-rotation transitions from the ground and low-lying electronic states, namely, $X^1\Sigma^+$, $a^3\Pi$, and $A^5\Delta$. From the inspection of Fig. 3(b), between 4200 cm^{-1} and 10000 cm^{-1}, the absorption is governed by transitions from the first excited $a^3\Pi$ state to the $b^3\Pi$ state ($a^3\Pi \rightarrow b^3\Pi$, the green line). The visible region from 10000 cm^{-1} to 17000 cm^{-1} is dominated by the strong, discrete band of the $X^1\Sigma^+ \rightarrow A^1\Sigma^+$ transition. Extending into the near-ultraviolet, from 17000 cm^{-1} to 30000 cm^{-1}, a series of broader features arise primarily from the $a^3\Pi \rightarrow d^3\Pi$ transitions. The concurrent strength of both singlet and triplet transitions in the visible to near-UV underscores the critical

spectroscopic role of the quasi-degenerate $a^3\Pi$ state, consistent with its predicted dominant ground-state character when spin–orbit coupling is considered.

At higher energies (> 30000 cm^{-1}) in Fig. 3(b), the absorption profile transitions into a strong, quasi-continuous background. This UV opacity is overwhelmingly dominated by transitions within the quintet manifold. A particularly broad and pronounced feature in this region arises from the $A^5\Delta \rightarrow B^5\Delta$ transition. The high density of quintet states, coupled with their non-negligible thermal population at 2000 K, results in a multitude of overlapping transitions that collectively smear into a continuum, defining the long-wavenumber opacity of OsO at high temperature.

Unlike in molecules of lighter elements such as ZrO,[12] where the visible spectra are predominantly contributed by transitions between singlet states (e.g., $X^1\Sigma^+ \rightarrow B^1\Pi$), the high-temperature opacity of OsO is much more complicated, which is a composite of three distinct spin manifolds. It arises from the concurrent intensity of singlet transitions ($X^1\Sigma^+ \rightarrow A^1\Sigma^+$), the high density of triplet transitions originating from the low-lying $a^3\Pi$ reservoir, and — most distinctively — the continuum-forming effect due to overlapping high-spin quintet transitions. This quintet-driven UV continuum represents a unique spectral signature of OsO among early transition-metal diatomics.

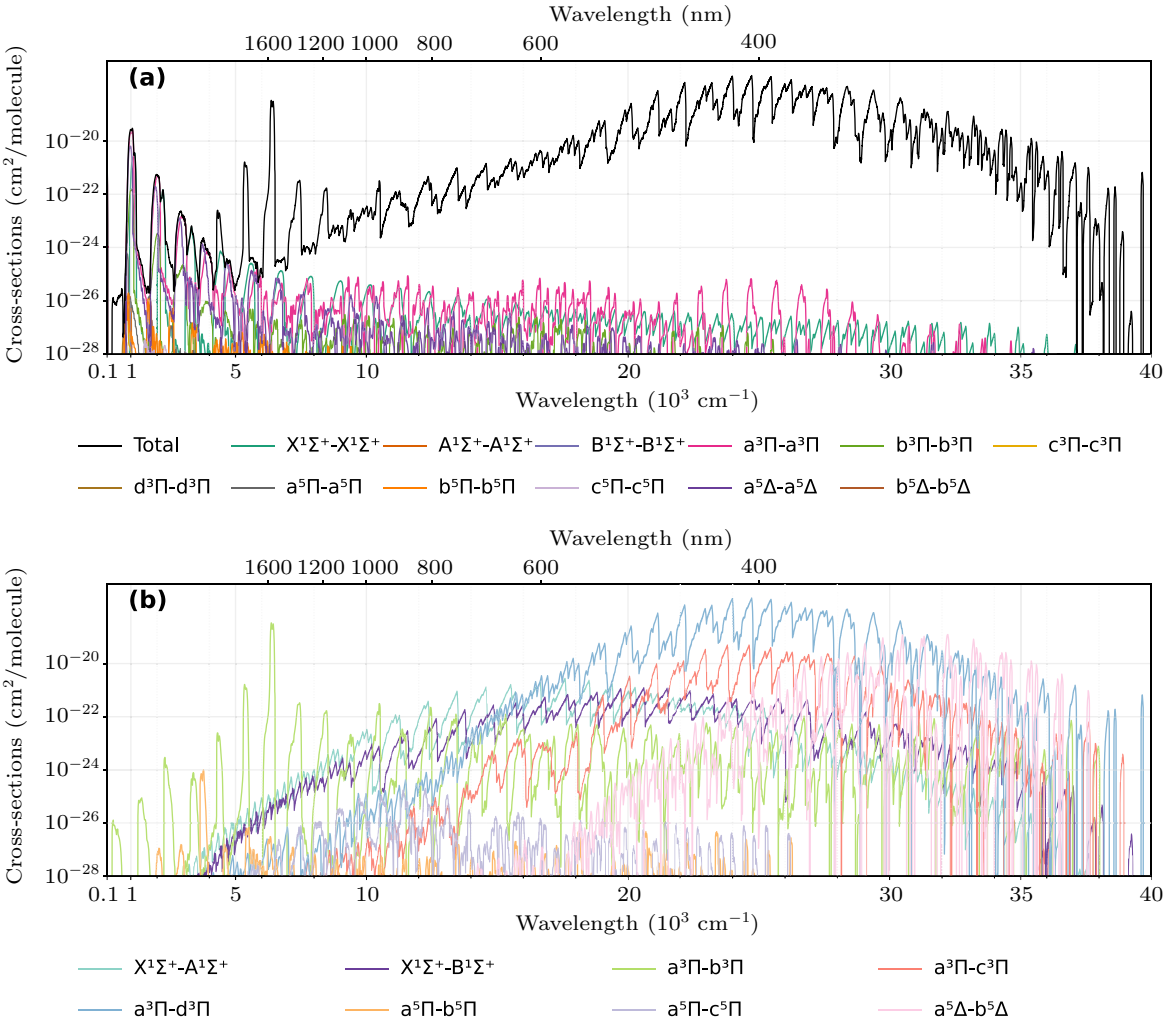


Fig. 3. Absorption cross sections of OsO at a temperature of 2000 K. In panel (a), contributions in 100–4000 cm^{-1} are presented which are predominantly caused by vibration-rotation transitions within individual electronic states. In panel (b), contributions from electronic (vibronic) transitions between different electronic states are shown. The total OsO absorption cross sections are represented by black-solid lines in panel (a). All rotational levels with $J \leq 100$ are included.

Figure 4 presents the absorption cross section across 300 K, 1000 K, 2000 K, 3000 K, and 5000 K. The spectrum exhibits a pronounced thermal response, with distinct behaviors observed in different spectral regions that reflect the population distribution among electronic and rovibrational states.

At the lowest temperature of 300 K, the population is heavily concentrated in the ground state, leading to an absorption spectrum dominated by transitions originating from the $X^1\Sigma^+$ and $a^3\Pi$ states, i.e., $X^1\Sigma^+ \rightarrow X^1\Sigma^+$ in 1000–5000 cm^{-1}, $X^1\Sigma^+ \rightarrow A^1\Sigma^+$ in 5000–15000 cm^{-1}, and $a^3\Pi \rightarrow d^3\Pi$ in the region above 15000 cm^{-1}. As the temperature increases to 1000 K and subsequently to 2000 K, a significant enhance-

ment in absorption intensity is observed across the low- to mid-infrared region (100–20000 cm^{-1}). This enhancement is attributed to the increased thermal population of excited electronic and rovibrational levels, which activates a multitude of additional transition pathways. These newly accessible transitions effectively fill in the spectral gaps present at 300 K, while simultaneous line broadening effects cause the discrete rovibrational structures to merge into broader spectral features.

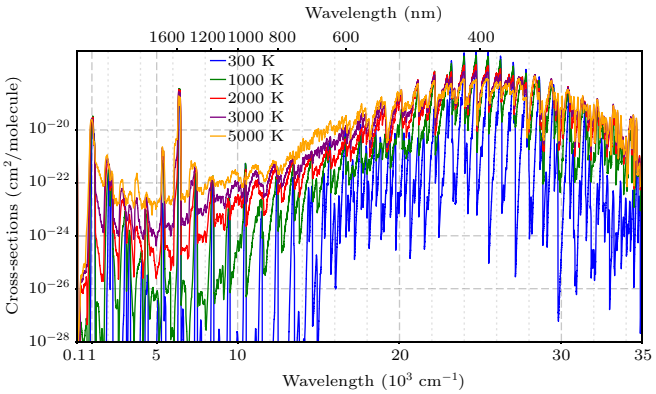


Fig. 4. The total OsO absorption cross sections at several temperatures.

The most dramatic change occurs between 300 K and 2000 K. At 2000 K, the absorption in the 100–20000 cm^{-1} range increases by several orders of magnitude and develops a quasi-continuous envelope, a consequence of the superposition of numerous broadened lines from densely populated excited states. This trend continues at 3000 K and 5000 K, where the absorption envelope further intensifies and smooths. In contrast, the high-energy ultraviolet region (20000–40000 cm^{-1}) exhibits a comparatively subdued response to temperature increase. In this region, the spectra are greatly broadened at high temperatures and form a strong quasi-continuous background. Our calculation of the potential energy curves for all 12 electronic states provides an indispensable foundation for accurately simulating the complete spectral characteristics — from a structured spectrum dictated mainly by low-lying state populations at lower temperatures to a continuous absorption dominated by highly excited states at high temperatures.

5. Conclusion

In conclusion, we have conducted the first comprehensive theoretical investigation of the opacity of OsO over the astrophysically crucial 300–5000 K range. The primary outcome of this work is the creation of a high-quality, reusable dataset, which includes complete line lists and absorption cross-sections for OsO. By combining high-accuracy relativistic electronic structure theory, we have computed a complete line list and the associated absorption cross-sections. Our analysis of this dataset reveals that the opacity of OsO is fundamentally shaped by its dense manifold of low-lying electronic states. A key feature is the near-degeneracy of the $X^1\Sigma^+$ and $a^3\Pi$ states, which leads to significant populations in both states even at moderate temperatures. Consequently, at 2000 K, the absorption spectrum emerges as a composite from three distinct spin manifolds: it is characterized by strong singlet transitions (notably $X^1\Sigma^+ \rightarrow A^1\Sigma^+$), numerous triplet transitions originating from the $a^3\Pi$ reservoir, and a distinctive UV continuum formed by the overlap of quintet-state transitions. The radiative opacities at temperatures of 300–5000 K are demonstrated. This dataset fills a critical gap in spectroscopic databases by providing the first high-temperature opacity data for OsO. The generated line list and cross-sections establish a foundation for interpreting potential OsO signatures in astrophysical spectra, particularly in r-process enriched environments such as kilonovae and metal-poor stars. These data will facilitate future spectroscopic searches for heavy-element molecules and help constrain nucleosynthetic conditions in extreme astrophysical events. We anticipate that this resource will be of significant value to the astrophysics and molecular physics communities. We also plan to continuously expand the dataset by including other molecules relevant to astrophysical atmospheres in the future.

Data availability statement

The data presented in this paper are openly available in Science Data Bank at the following link https://doi.org/10.57760/sciencedb.j00113.00282.

Acknowledgments

Project supported by the Science Challenge Project (Grant No. TZ2025013) and the National Natural Science Foundation of China (Grant Nos. 12274384 and 12335015).

References

[1] Rogers F J and Iglesias C A 1994 *Science* **263** 50
[2] Bauche J, Bauche-Arnoult C and Peyrusse O 2006 *J. Quant. Spectrosc. Radiat. Transfer* **99** 55
[3] Bailey J E, Nagayama T, Loisel G P, *et al.* 2015 *Nature* **517** 56
[4] Zeng J L, Gao C, Liu P F, *et al.* 2022 *Science China* **65** 53
[5] Tennyson J and Yurchenko S N 2017 *Mol. Astrophys.* **8** 1
[6] Johnson J A 2019 *Science* **363** 474
[7] Cowan J J, *et al.* 2021 *Rev. Mod. Phys.* **93** 015002
[8] Thielemann F K, Eichler M, Panov I V and Wehmeyer B 2017 *Annu. Rev. Nucl. Part. Sci.* **67** 253
[9] Avila J N, Lugaro M, Ireland T R, *et al.* 2012 *Astrophys. J.* **744** 49
[10] Schwenke D W 1998 *Faraday Discuss.* **109** 321
[11] Bowesman C A, Qu Q, McKemmish L K, *et al.* 2024 *Mon. Not. R. Astron. Soc.* **529** 1321
[12] Perri A N, Taher F and McKemmish L K 2023 *Mon. Not. R. Astron. Soc.* **524** 4631
[13] Bernath P F, Dodangodage R and Liévin J 2022 *Astrophys. J.* **933** 99
[14] Bernath P F, Dodangodage R and Liévin J 2023 *Astrophys. J.* **953** 181
[15] Yurchenko S N, Brady R P, Tennyson J, *et al.* 2023 *Mon. Not. R. Astron. Soc.* **527** 4899

[16] Liu W J and Peng D L 2009 *J. Chem. Phys.* **131** 031104
[17] Tennyson J, Yurchenko S N, Al-Refaie A F, *et al.* 2016 *J. Mol. Spectrosc.* **327** 73
[18] Tennyson J and Yurchenko S N 2018 *Atoms* **6** 26
[19] Gordon I E, Rothman L S, Hill C, *et al.* 2017 *J. Quant. Spectrosc. Radiat. Transfer* **203** 3
[20] Gordon I E, Rothman L S, Hargreaves R J, *et al.* 2022 *J. Quant. Spectrosc. Radiat. Transfer* **277** 107949
[21] Jacquinet-Husson N, Armante R, Scott N A, *et al.* 2016 *J. Mol. Spectrosc.* **327** 31
[22] Delahaye T, Armante R, Scott N A, *et al.* 2021 *J. Mol. Spectrosc.* **380** 111510
[23] Voigt W 1912 *Sitzungsber. Bayer. Akad. Wiss. Math.-Naturwiss. Kl.* **25** 603
[24] Vidler M and Tennyson J 2000 *J. Chem. Phys.* **113** 9766
[25] Kato H 1993 *Bull. Chem. Soc. Jpn.* **66** 3203
[26] Pack R T and Hirschfelder J O 1968 *J. Chem. Phys.* **49** 4009
[27] Rothman L S, Gordon I E, Barber R J, *et al.* 2010 *J. Quant. Spectrosc. Radiat. Transfer* **111** 2139
[28] Peng D and Reiher M 2012 *Theor. Chem. Acc.* **131** 1081
[29] Zobel J P, Widmark P O and Veryazov V 2020 *J. Chem. Theory Comput.* **16** 278
[30] Zobel J P, Widmark P O and Veryazov V 2021 *J. Chem. Theory Comput.* **17** 3233
[31] Angeli C, Borini S, Cestari M and Cimiraglia R 2004 *J. Chem. Phys.* **121** 4043
[32] Zhang Y, Suo B B, Wang Z K, *et al.* 2020 *J. Chem. Phys.* **152** 064113
[33] Yan W and Zou W L 2023 *Chin. Phys. B* **32** 113101
[34] Tennyson J, Hill C and Yurchenko S N 2013 *AIP Conference Proceedings* **1545** 186